Journal of Sound and Vibration (2001) **243**(5), 797–821
doi:10.1006/jsvi.2000.3432, available online at http://www.idealibrary.com on IDEAL®

MEASUREMENT TECHNIQUE TO ASSESS THE ACOUSTIC PROPERTIES OF A SILENCER COMPONENT FOR TRANSIENT ENGINE CONDITIONS

D. C. Van Der Walt

Bosal Africa, Automotive, Research and Development, P.O. Box 1652 *Pretoria* 0001, *South Africa.*
E-mail: danievdw@bosal.co.za

(*Received* 27 *January* 2000, *and in final form* 9 *August* 2000)

This paper describes the development and validation of procedures for measuring the acoustic properties of an individual component of an exhaust system on a test bed under engine acceleration representing realistic operating conditions. However, collection of such data requires reliable induct pressure measurements where the contamination of the acoustic pressure field by shear layer turbulence and other hydrodynamic disturbances [1] make this a formidable challenge. The technique was first developed and optimized on a cold flow bench to simulate partly the acoustic conditions during engine acceleration, before applying it to an actual vehicle. Bench test results showed that order analysis measurement techniques can be employed to evaluate the acoustic performance of a silencer component for variable harmonic excitation in the presence of mean flow. The additional factors concerned in performing measurements on the test bed are illustrated by some preliminary measurements.

1. INTRODUCTION

The automotive industry is placing an increasing demand on exhaust system suppliers to reduce development lead times, while the increasing environmental demands place severe legislative constraints on drive-by and proximity targets. Therefore, it has now become an essential requirement to follow a rational design strategy based on predictive modelling followed by experimental assessment of orifice noise emissions for both the exhaust silencer components and the complete system, to ensure rapid and cost-effective exhaust system development.

Currently, tail-pipe orifice noise emission is measured during controlled acceleration and deceleration of the engine on a chassis or engine dynamometer, to evaluate and then refine the acoustic performance of the exhaust system for the practical operating conditions of the engine. The results are generally presented in a Campbell diagram which displays the frequency content of tail-pipe noise. Figure 1 shows such a tail-pipe noise measurement which was recorded for a full throttle run up on a chassis dynamometer. The radial straight lines that increase with frequency and engine speed can be identified as order noise, generated by the cyclic pulsating flow through the valves. The wave motion is periodic in nature and the exhaust noise signature consists of narrow band components harmonically related to the firing frequency of the engine and are expressed as multiples of the engine rotational speed. The signature also includes contributions from flow noise, represented by the broad band noise above 300 Hz. Flow noise is caused by turbulence and other

0022-460X/01/250797 + 25 $35.00/0

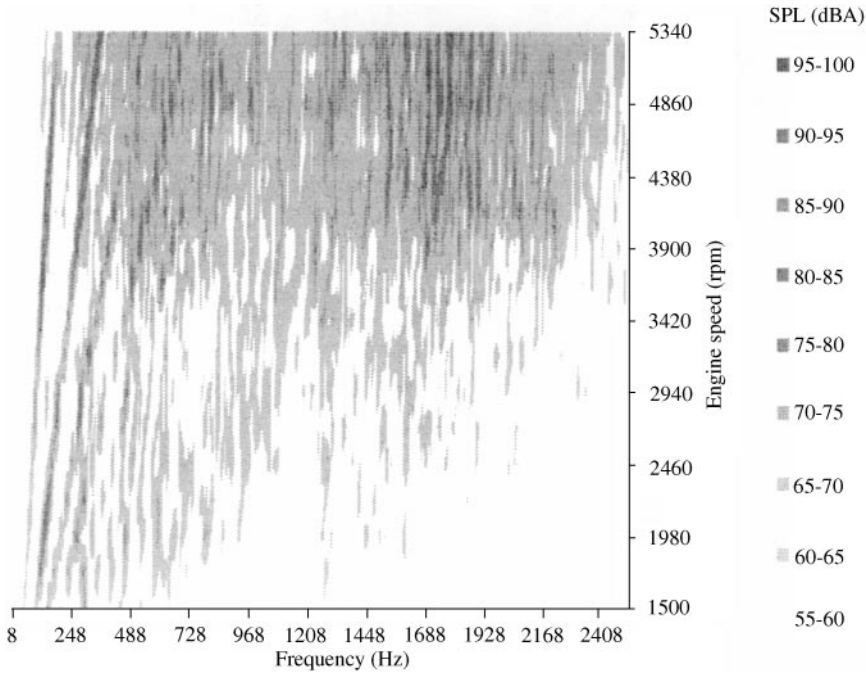

Figure 1. Campbell diagram of a tail-pipe noise measurement recorded for a full throttle run-up.

flow-induced aeroacoustic sources at expansions, contractions, bends and the tail-pipe outlet [1].

The exhaust system is assembled from a number of elements consisting of chambers and connecting pipes, etc., which interact dynamically. The overall performance of such reactive systems is governed by system resonances which depend on the resonances of individual elements [2]. The quarter and half wave length resonance frequencies can be related to the effective lengths of the connecting pipes with their boundary conditions and the cavity resonances are related to the chamber volume with the connecting pipe length and diameter of each individual element. In order to optimize the acoustic performance of the design it is essential to ensure that the resonance frequencies of these components do not coincide, but are well separated. Therefore, it is essential to obtain a clear understanding of the contribution of each individual element to the overall acoustic performance of the complete exhaust system under practical operating conditions [2]. Assessment of tail-pipe noise measurements normally does not provide sufficient information to indicate the appropriate changes to each specific element that are required to optimize the acoustic performance of the complete exhaust system. Also, these measurements do not provide sufficient information to identify flow noise sources distributed along the system.

This paper presents new measurement technology that evaluates the acoustic performance of individual exhaust silencer components by using pairs of flush wall mounted pressure transducers at the inlet and outlet of each element or silencer box for the practical operating conditions of the engine. Although there exists an extensive literature on the acoustic modelling of exhaust systems and its validation, only a limited number of the relevant papers describe experimental measurements on a running engine. These have normally been restricted to constant speed measurements [3–6] where the time taken to obtain stable acoustic and temperature conditions for reliable measurements make this approach tedious and of limited practical application. Although constant speed engine

measurements may be sufficient to validate acoustic models, they do not represent the practical operating conditions of the engine. Appropriate assessment of the acoustic performance of individual silencer components, or of systems, should include the influence of engine speed and load and the corresponding variation in gas temperature distribution and mass flow that have a controlling influence on the spectral characteristics of the sources of excitation of the exhaust system and of its acoustic response. It is, therefore, essential to perform the measurements during engine acceleration or deceleration to provide sufficiently realistic descriptions of acoustic behaviour.

Before performing tests on a running engine, a first step has been the development of a measurement technique on a cold bench test with constant mean flow and variable harmonic excitation to simulate partly the acoustic conditions during engine acceleration. A wave decomposition method was used to calculate the positively and negatively travelling component waves at the inlet and outlet of a silencer box. Different order analysis techniques were investigated and order tracking was found to be best suited to capture the harmonic pressure time history. A precise estimation of the transfer functions at the inlet and outlet of a silencer component is essential to yield reliable results for the wave component evaluation. Measurement of transfer functions in the presence of mean flow is fraught with difficulty due to the reduced signal-to-noise ratios [7, 8]. Therefore, it was essential first to optimize the order tracking signal processing parameters to improve the reliability of the measurement. The importance of a relative calibration of the pressure transducers was also emphasized.

The measurement technique was then used to measure the acoustic performance of a simple expansion chamber on a cold bench test in the presence of mean flow. Measurements were compared to predictions performed with a validated numerical code to validate the technique. These are described in section 3. Following this, the measurement method was applied to the exhaust system of a 1·5 l, four-stroke, four-cylinder engine described in section 4. For simplicity, the acoustic performance of an expansion chamber was again evaluated for a practical acceleration run-up of the vehicle on a chassis dynamometer. The variable mass flow, engine rotational frequency and exhaust temperatures were recorded at regular intervals to provide the additional data required to perform the corresponding acoustic predictions. Measurements were compared to predictions performed with an extended version of the numerical code to determine if linear acoustic theory remains valid for running engines. A final discussion appears in section 5.

2. DEVELOPMENT OF THE MEASUREMENT METHOD

The measurement of radiated tail-pipe noise with order analysis techniques is common practice in the automotive industry; however, the evaluation of the wave components inside the exhaust system for the practical operating conditions of the engine has not yet been published, according to the author's knowledge. Swept sine excitation was adopted by Holland and Davies [8] to measure the acoustic power flux in flow ducts. They showed how this improved the reliability of the measurements in the presence of flow noise by improving the signal-to-noise ratio during the analysis of the data. This provided a useful basis for the measurement technology discussed here. However, some fundamental changes were required in the application of the method to measurements on a running engine. For example, the higher harmonics of exhaust noise require much faster sweep rates; therefore the analysis for the proposed measurement technique was optimized to produce reliable results for the first four harmonics.

2.1. BENCH TEST SET-UP

The bench test set-up is displayed in Figure 2. The silencer component and tubes containing the pressure transducer holders were placed inside a semi-anechoic chamber. Acoustic excitation was provided by means of a compression driver and the excitation signal was generated with a sweep functional generator. Air flow was controlled by an adjustable valve connected to a 6 bar line pressure. The rig is also provided with a water trap and a preliminary silencer to attenuate noise caused by the flow before it reaches the system under test. The measurements were performed in the presence of mean flow at a practically representative constant exhaust mass flow for a small four-cylinder engine at high engine speed, typically a mass flow of 0·07 kg/s was required to obtain a Mach number $M = 0{\cdot}1$ at 20°C.

The sound pressure time-history was measured with Kistler (Type 701A) quartz pressure transducers. The wide dynamic range (0–250 bar) and high sensitivity (80 ρC/bar) of the transducers make them suitable for these dynamic pressure measurements. The transducers were mounted flush behind a 2 mm hole in the pipes to reduce the effect of flow induced noise [8] as displayed in Figure 3. Charge amplifiers were used to produce a voltage output

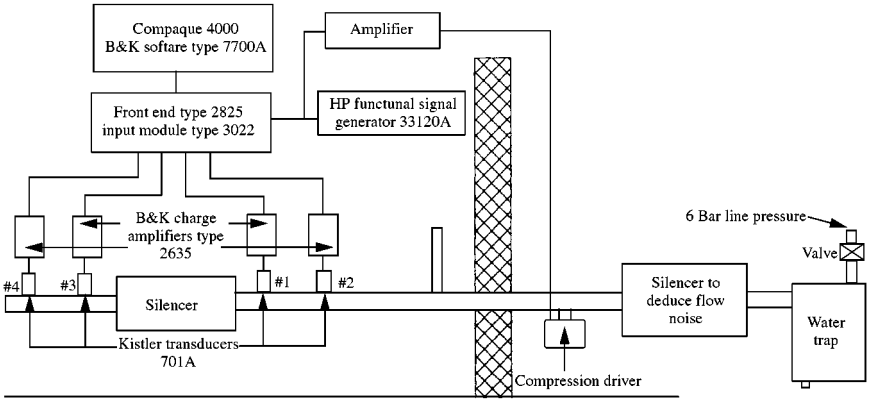

Figure 2. Bench test set-up.

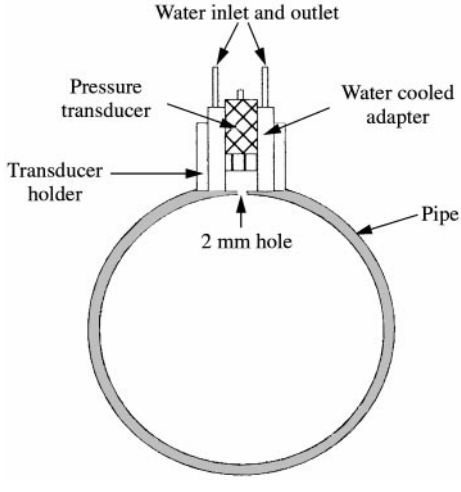

Figure 3. Pressure transducer installation.

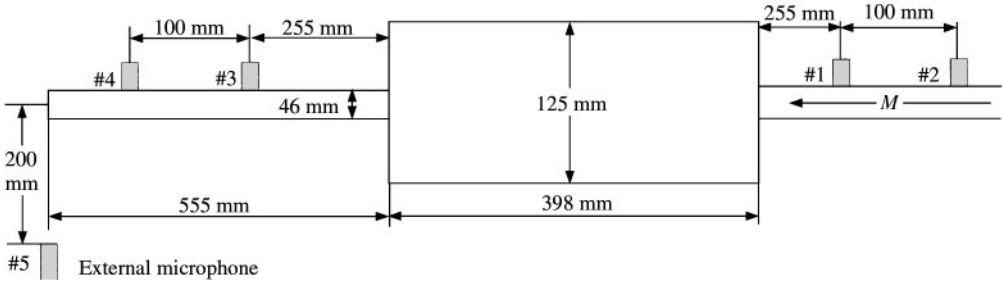

Figure 4. Simple expansion chamber.

signal proportional to the input charge of the transducers and a 100 mm transducer separation distance was used.

A simple expansion chamber was used for the experiments; the dimensions, direction of flow and the position of the pressure transducers in the inlet and outlet pipe and external microphone are indicted in Figure 4. The expansion chamber consists of a 2 mm thick shell with 1·5 mm end caps while the inlet and outlet pipes have a wall thickness of 2 mm. The expansion chamber radius was 62·5 mm giving an area expansion ratio between the pipe and the chamber of 7·38, which produces an estimated maximum attenuation of 20 log 7·38 or 17·3 dB. The first circumferential mode propagates when the Helmholtz number ka exceeds the value of 1·84 [9]; hence the lowest higher order modes can only propagate in the chamber at frequencies above 1600 Hz.

2.2. WAVE DECOMPOSITION CALCULATIONS

The wave decomposition method has been the subject of extensive study and the method has been developed as a reliable and robust tool to validate the acoustic performance of silencer components for stationary bench test conditions. Bento Coelho [10] used the method to determine the incident wave attenuation and the upstream reflection coefficient of perforated resonators for stationary bench test conditions. The application of the four-microphone wave decomposition method was also extensively described in a paper by Davies *et al.* [11] and used to validate the linear acoustic models of multiple path silencers with random excitation and mean flow. Holland [8] suggested some further refinements to the signal processing for the method, which will be adopted for this study.

The wave components are determined from the auto-spectra, cross-spectra and transfer functions between two pairs of microphones placed at the inlet and outlet side of the silencer component. Pressure ratios, reflection coefficients, acoustic impedence, attenuation, and power flux spectra may be estimated from the complex values of the two wave components. With reference to Figure 4, at each frequency the wave components (P^+ and P^-) at the inlet and outlet side are calculated from the corresponding pressure measurements (P_1–P_4) to characterize the acoustic performance of the system. At the inlet side of the system, the acoustic pressure at any plane can be related to the wave components at station $\#1$.

Thus, with one-dimensional waves,

$$\hat{P}_x(\omega, x) = \hat{P}_1^+ e^{i\hat{k}^+ x} + \hat{P}_1^- e^{i\hat{k}^- x}, \tag{1}$$

where the symbol, $\hat{}$ over a quantity indicates that it is complex and the distance x is determined relative to station $\#1$.

Hence

$$\hat{P}_1(\omega, x) = \hat{P}_1^+ + \hat{P}_1^- \quad \text{for} \quad x = 0, \tag{2}$$

and

$$\hat{P}_2(\omega, x) = \hat{P}_1^+ \, \mathrm{e}^{-\mathrm{i}\hat{k}^+ l} + \hat{P}_1^- \, \mathrm{e}^{\mathrm{i}\hat{k}^- l} \quad \text{for} \quad x = -l. \tag{3}$$

The complex wave number ($\hat{k}$) is defined by

$$\hat{k} = \frac{\omega}{c} - \mathrm{i}a, \qquad \hat{k}^+ = \frac{\hat{k}}{(1+M)}, \qquad \hat{k}^- = \frac{\hat{k}}{(1-M)}, \tag{4a, b, c}$$

where M is the mean flow Mach number, a is the visco-thermal attenuation coefficient [8] and c is the speed of sound.

The auto-spectrum ($C_{1,1}$) at station $\#1$ is defined by

$$C_{1,1} = (\hat{P}_1^+ + \hat{P}_1^-)(\hat{P}_1^+ + \hat{P}_1^-)^*, \tag{5}$$

where * represents the complex conjugate.

The cross spectrum ($C_{2,1}$) between stations $\#2$ and $\#1$ is defined by

$$\hat{C}_{2,1} = (\hat{P}_1^+ \mathrm{e}^{-\mathrm{i}\hat{k}^+ l} + \hat{P}_1^- \mathrm{e}^{\mathrm{i}\hat{k}^- l})(\hat{P}_1^+ + \hat{P}_1^-)^* \tag{6}$$

and the reflection coefficient at the inlet side is expressed by

$$\hat{R}_1 = \hat{P}_1^- / \hat{P}_1^+, \tag{7}$$

hence

$$\frac{\hat{C}_{2,1}}{C_{1,1}} = \frac{\mathrm{e}^{-\mathrm{i}\hat{k}^+ l} + \hat{R}_1 \mathrm{e}^{\mathrm{i}\hat{k}^- l}}{1 + \hat{R}_1}, \qquad \hat{R}_1 = -\left(\frac{\hat{C}_{2,1} - C_{1,1}\mathrm{e}^{-\mathrm{i}\hat{k}^+ l}}{\hat{C}_{2,1} - C_{1,1}\mathrm{e}^{\mathrm{i}\hat{k}^- l}}\right), \qquad \hat{R}_1 = -\left(\frac{\hat{H}_{2,1} - \mathrm{e}^{-\mathrm{i}\hat{k}^+ l}}{\hat{H}_{2,1} - \mathrm{e}^{\mathrm{i}\hat{k}^- l}}\right), \tag{8–10}$$

where $\hat{H}_{2,1} = \hat{P}_2 / \hat{P}_1$ is the transfer function between the signals at stations, $\#2$ and $\#1$.

From equation (5),

$$C_{1,1} = (P_1^+)^2 (1 + \hat{R}_1)(1 + \hat{R}_1)^*. \tag{11}$$

Therefore, it follows that the modulus of the incident wave component at station $\#1$ is

$$\hat{P}_1^+ = \sqrt{C_{1,1}} / |(1 + \hat{R}_1)| \tag{12}$$

and the complex reflected wave component at station $\#1$ is defined by

$$\hat{P}_1^- = \hat{R}_1 \hat{P}_1^+. \tag{13}$$

Upon noting that the phase of P_1^+ is chosen to be zero, equation (12) also gives the modulus of P_1^+.

The same procedure is followed to determine the wave components at the outlet side of the silencer component (stations $\#3$ and $\#4$) with station $\#3$ as the reference.

The phase relationship between stations # 3 and #1 relative to station #1 can be estimated from the cross-spectrum ($\hat{C}_{3,1}$) between stations #3 and #1 [8], in order to determine the complex value of P_3^+:

$$\hat{P}_3^+ = P_3^+ \left(\frac{\hat{C}_{3,1}}{(\hat{P}_3^+ + \hat{P}_3^-)(\hat{P}_1^+ + \hat{P}_1^-)^*} \right). \tag{14}$$

A software program was developed to calculate the wave components from the measured acoustic quantities and the temperature and mass flow conditions.

The acoustic field inside a mechanical silencer component is highly reactive; hence the acoustic power flux for a certain position and frequencies may be very close to zero due to the small difference between the forward travelling wave and the reflected wave amplitudes. Therefore, a precise relative calibration of the pressure transducers is critical for the success of the measurement technique [8]. The relative calibration was performed by exposing the pressure transducers to the same pressure field and the relative calibration factors were estimated from the following transfer functions:

$$\hat{H}_{n,1} = \frac{\hat{P}_n \hat{P}_1^*}{\hat{P}_{1,1}}, \tag{15}$$

where $\hat{P}_n \hat{P}_1^*$ is the cross-spectrum, $\hat{P}_{1,1}$ the auto-spectrum, $n = 2$–4, and * is the complex conjugate.

2.3. ORDER ANALYSIS TECHNIQUES

The application of the measurement procedure involves the choice of a number of vital parameters. In contrast to normal stationary signal analysis, one now must take due account of the fact that one has non-stationary signal records. The basic engine cycle frequency, the mass flow and temperature are all changing systematically in time, at some sweep rate which is also never quite stationary. As noted earlier one wishes to extract the spectral characteristics of the time-varying signal at specific engine speed intervals to describe the acoustic quantities. Order analysis is a standard measurement technique which is tailored to extract the harmonic component information of a measurement from an acoustic-mechanical system under periodic loading [12]. Therefore, it is ideally suited to capture the exhaust noise harmonic pressure information at the four pressure transducer stations during a run-up or run-down of the engine. Order analysis methods are commonly divided into two basic groups: fixed sampling rate methods and order tracking methods [13].

The fixed sampling rate method uses a fixed sampling rate and the Fourier transform of each record gives the corresponding frequency spectrum. Measurement of the spectrum at appropriate fixed steps in rotation speed of the engine gives the well-known Campbell diagram (see Figure 1), where the signature spectra are plotted against engine speed [14]. Here the harmonic components appear as radial straight lines and system resonances appear as fluctuations in amplitude along vertical straight lines; the spectral amplitudes may be indicated by a colour scale. Smearing of the higher order components, is, however, a natural consequence of the fixed rate sampling. Each record is acquired for the same fixed time interval, while the corresponding sweep rate of individual harmonics (orders) increases with the order number over that time interval, so that the energy of the order is smeared over a number of analysis lines [13, 14]. Leakage is also introduced when the time signal contains a non-integer number of periods within the record length [15].

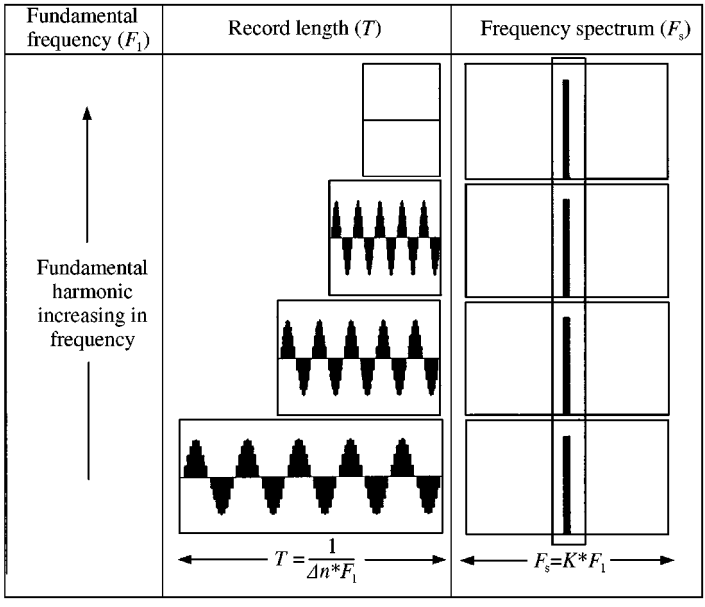

Figure 5. Example of the order tracking performed on the fundamental harmonic, increasing in frequency and the resultant updating of the record length and the frequency spectrum with the fundamental harmonic located on the same analysis line.

Order tracking uses the instantaneous engine rotation speed to synchronize the sampling frequency with the fundamental frequency, normally the firing frequency. Therefore, the time record is measured in revolutions rather than seconds and the corresponding FFT spectrum is measured in orders rather than frequency [14]. The result is a high-resolution order-spectrum and the power of each harmonic component is concentrated in an individual line, avoiding smearing. The time signals are also forced to contain an integer number of periods within the record length, hence as a result of this combination leakage is eliminated [15]. Figure 5 illustrates the update of the frequency span, record length and frequency resolution for each measurement interval.

The following equations define the basic fundamentals of order tracking [13],

$$F_s = Kf_1, \qquad \Delta f = \Delta n f_1, \qquad T = \frac{1}{\Delta n f_1}. \tag{16–18}$$

Here F_s is the frequency span (Hz), proportional to r.p.m., f_1 the fundamental frequency (Hz), proportional to r.p.m., K the number of orders in the analysis, constant, T the record length (seconds), inversely proportional to r.p.m., Δf the frequency resolution (Hz), proportional to r.p.m., and Δn the order resolution, (orders), constant.

2.4. ANALYSIS METHOD AND OPTIMIZATION

The analysis was performed with a B&K Pulse multi-channel system and the order tracking method was used for the reasons discussed in section 2.3. The fundamental harmonic of the excitation signal was used as a tachometer signal and the first four order components were extracted. The analysis was performed with a Hanning window, 75%

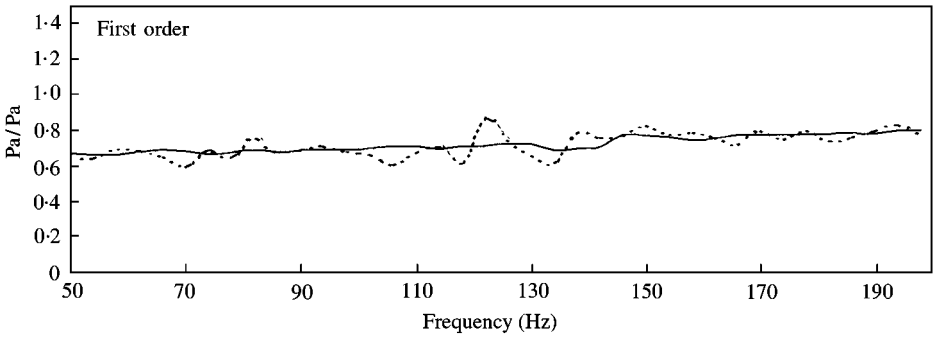

Figure 6. Real part of the transfer function $H_{4,3}$ for the $2E$ component analyzed with a 0·2 order resolution without averaging (dashed) and 0·025 order resolution with averaging (solid) for a Mach number of 0·1.

overlap, exponential averaging and order spectra were captured at 4 Hz intervals of the fundamental or firing frequency.

On the test bench, the exhaust noise harmonics can either be simulated with a sweep-ramp signal and analyzed simultaneously, or each harmonic order can be individually simulated with a sine-sweep signal. Sine-sweep excitation was preferred because higher excitation levels can be achieved with lower amplification, which improves the signal-to-noise ratio and enhances the durability of the compression driver. The acoustic excitation for a four-cylinder, four-stroke engine was simulated between 1500 and 6000 r.p.m.; hence, the fundamental harmonic of exhaust noise is $2 \times$ *engine rotation frequency* ($2E$) and covers the frequency range from 50 to 200 Hz. A linear sweep rate of 0·5 Hz/s (15 r.p.m./s) was used for the fundamental frequency. Linear engine sweep rates between 15 and 30 r.p.m./s (0·5 and 1 Hz/s for the fundamental frequency for a four-cylinder, four-stroke engine) are realistic for a practical runup of an engine.

Signal-to-noise ratios are reduced when measurements are performed in the presence of mean flow due to the increase in the broadband background noise levels; hence, it is more difficult to obtain reliable measurements. To illustrate the effect of order resolution and averaging, the real part of the transfer function $H_{4,3}$ (see Figure 6) in the outlet pipe was evaluated. A theoretical transfer function $H_{4,3}$ produces a smooth horizontal curve for the first harmonic component due to the absence of acoustic resonance. This was the case when the analysis was performed with an order resolution of 0·025 orders and 10 averages compared to the spiky appearance of the bigger 0·2 orders resolution measurement without averaging. The coherence (see Figure 7) and the signal-to-noise ratio (see Figure 8) were also improved when the order tracking analysis was performed with the higher order resolution and averaging. The higher order resolution concentrates the acoustic energy of the order components in a narrower band and the averaging process then tends to suppress any random fluctuations of the harmonic components by reducing the relative levels of the broad band noise contributions. The signal-to-noise ratio was estimated from the ratio of the acoustic pressure with and without acoustic excitation in the presence of mean flow (Mach number $M = 0{\cdot}1$). It can also be observed from Figure 9 that the signal-to-noise ratios are generally higher in the inlet pipe at station $\#1$, compared to the outlet pipe at station $\#3$. This is due to the attenuation of the harmonic components by the expansion chamber in combination with the flow-induced noise at the outlet of the expansion chamber.

One problem associated with harmonic excitation is the increasing sweep rate required at the higher harmonics and the possibility of smearing of the higher order components. With

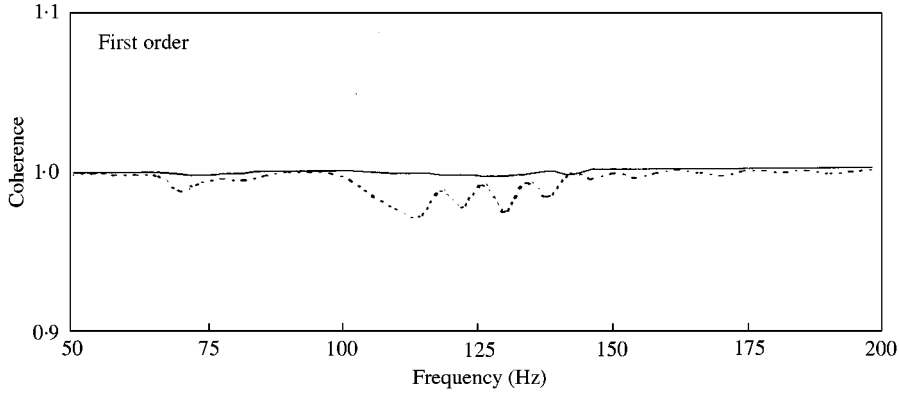

Figure 7. Coherence between station #4 and #3 for the 2*E* component analyzed with a 0·2 order resolution without averaging (dashed) and 0·025 order resolution with averaging (solid) for a Mach number of 0·1.

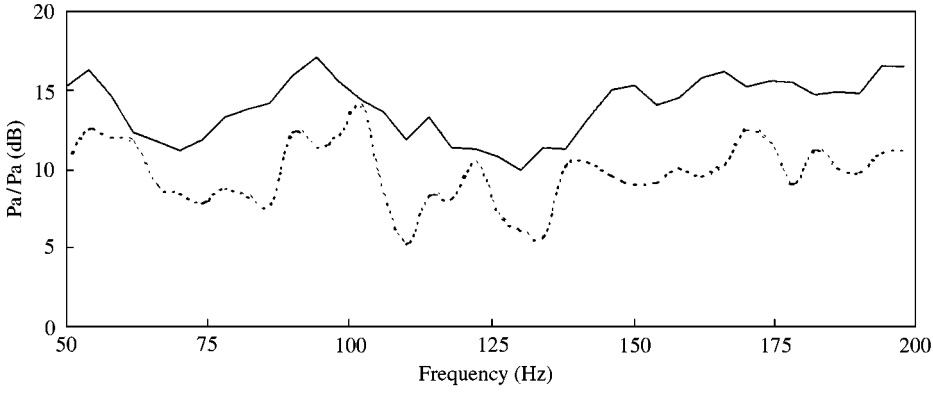

Figure 8. Signal-to-noise ratio at station #3 for the 2*E* component analyzed with a 0·2 order resolution without averaging (dashed) and 0·025 order resolution with averaging (solid) for a Mach number of 0·1.

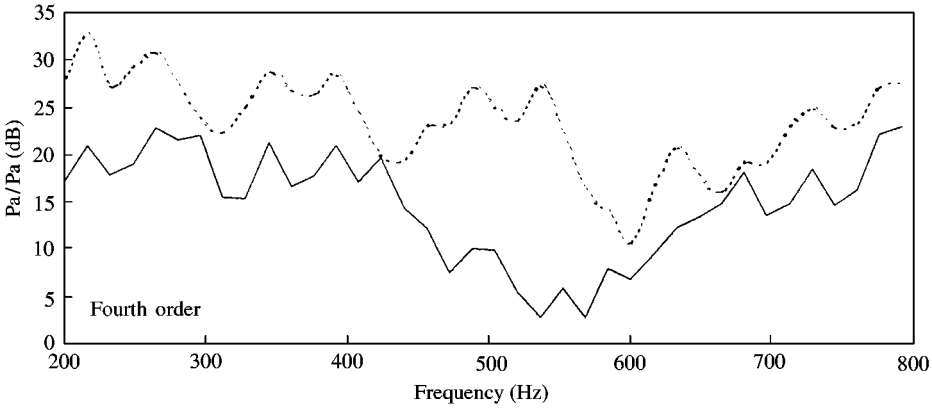

Figure 9. Signal-to-noise ratio at station #1 (dashed) and station #3 (solid) for the 8*E* component analyzed with a 0·025 order resolution and 10 averages for a Mach number of 0·1.

order tracking and a linear sweep rate this problem is eliminated, provided that the record length at the start of the measurement is smaller than the time taken to sweep the first measurement interval. The sampling frequency is the lowest at the start of the measurement and synchronised with the fundamental frequency. In practice a maximum number of 10 averages could be achieved with the 0·025 order resolution, while still avoiding smearing at the start of the measurement. Amplitude smearing also occurs for order tracking due to the increasing frequency range covered by the higher order components. Measurements were captured at 4 Hz intervals for the fundamental frequency hence, the corresponding $8E$ component covers a frequency range of 16 Hz for each interval. This was found to be adequate to describe the acoustic performance of the expansion chamber and a good compromise between measurement resolution and the corresponding number of averages available.

3. BENCH TEST MEASUREMENTS AND PREDICTIONS

The measurement technique developed in section 2 was then used to measure the acoustic performance of the expansion chamber displayed in Figure 4 on the cold flow bench displayed in Figure 2. Again, the acoustic excitation for a four-cylinder, four-stroke engine was simulated between 1500 and 6000 r.p.m. corresponding to a fundamental frequency ($2E$) from 50 to 200 Hz which was swept at 0·5 Hz/s. Measurements of transfer functions, system attenuation, normalized acoustic power flux, and normalized radiated power were compared to predictions to validate the technique.

3.1. ACOUSTIC PREDICTIONS

The prediction of the acoustic performance of the silencer component was performed with APEX (Acoustic prediction of exhaust systems), a linear acoustic software program [2] developed by Prof. P.O.A.L. Davies at the University of Southampton. The program provides the linear acoustic predictions of the pressure distribution and energy transport throughout an exhaust system of specific geometry [11, 16, 17]. Systems with complex geometries are modelled by means of a sequence of simple chambers and the program takes full account of the flow velocities and temperature distribution within the chambers and the complete system. The relative acoustic performance is described in single parameter spectrum format.

Constant mass flow and temperature conditions exist for the measurements on the bench, therefore the harmonic components at each measurement interval are subjected to the same conditions. Hence, the program was used in its standard format to calculate the acoustic performance for each order separately with the appropriate frequency range and measurement resolution.

3.2. RESULTS AND DISCUSSION

With reference to the expansion chamber in Figure 4, Figure 10 shows a comparison between the predicted and measured transfer function $H_{3,1}$ and Figure 11 shows the predicted and measured transfer function $H_{1,5}$ for the first four order components ($2E$, $4E$, $6E$ and $8E$) with a Mach number of 0·1. The external microphone for $H_{1,5}$ was positioned perpendicular and 200 mm from the centre of the tail-pipe outlet. At each frequency the transfer function $H_{3,1}$ was estimated from the ratio of the spectral acoustic pressure

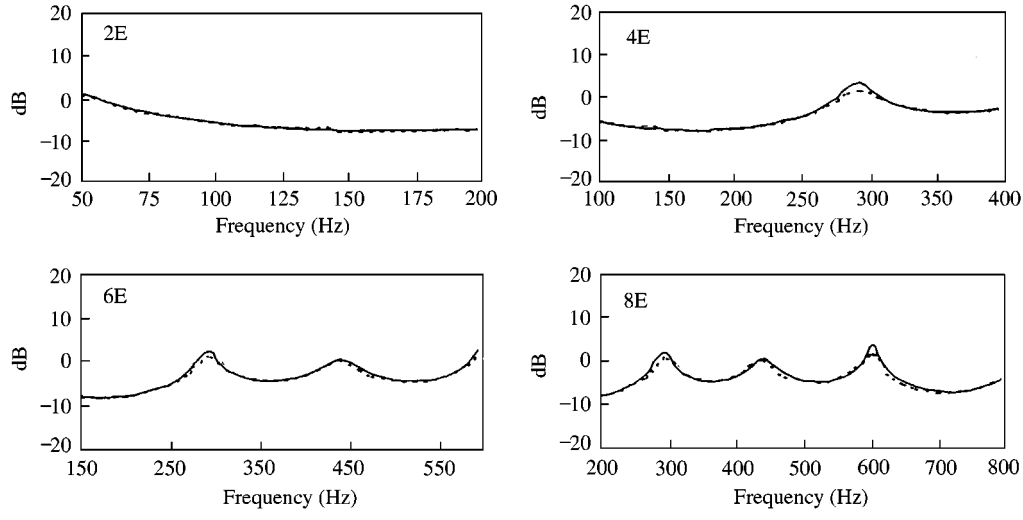

Figure 10. Measured (dash) and predicted (solid) magnitude of the transfer function $H_{3,1}$ with a Mach number of 0·1.

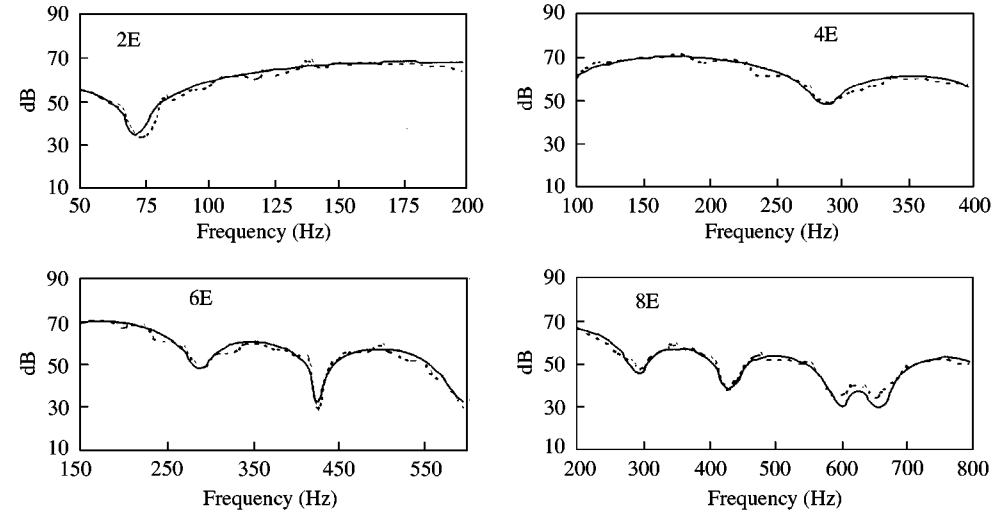

Figure 11. Measured (dash) and predicted (solid) magnitude of the transfer function $H_{1,5}$ with a Mach number of 0·1.

amplitudes at station #3 to that at station #1, while the transfer function $H_{1,5}$ was estimated from the cross-spectrum between stations #1 and #5 normalized by the auto-spectrum at station #5.

The system attenuation was estimated from the incident wave components at the inlet and outlet of the expansion chamber, so that

$$Att = 20 \log |P_1^+ / P_3^+|. \tag{19}$$

Figure 12 shows a comparison between the predicted and measured system attenuation for the first four order components with a Mach number of 0·1.

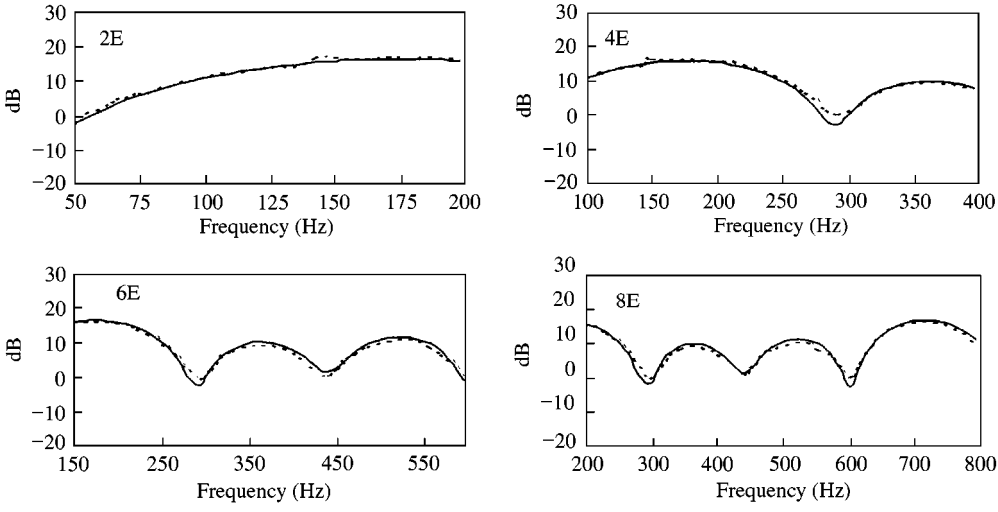

Figure 12. Measured (dash) and predicted (solid) system attenuation with a Mach number of 0·1.

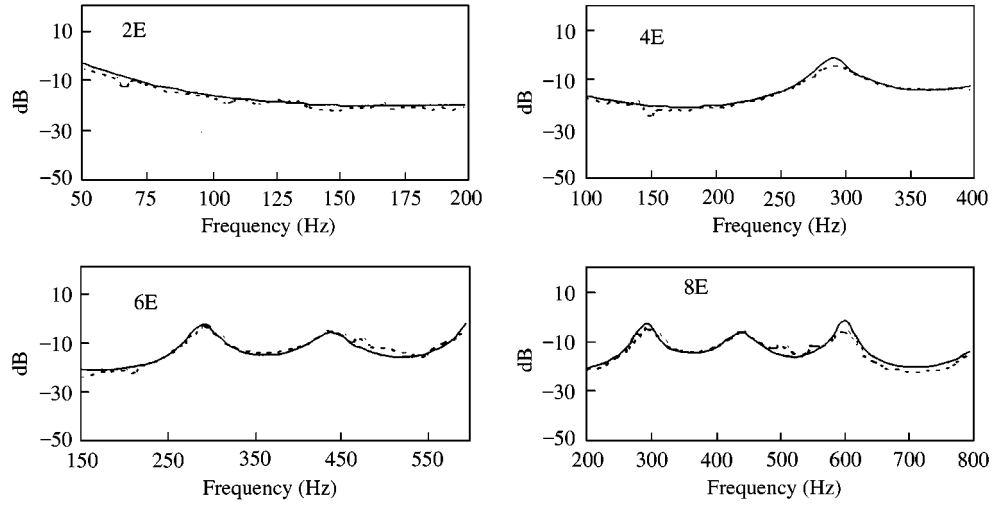

Figure 13. Measured (dash) and predicted (solid) normalized acoustic power flux in the outlet pipe with a Mach number 0·1.

The acoustic power flux in the outlet pipe was determined from the acoustic intensity I [16] and the corresponding pipe area. Thus, for example, at station #3,

$$I_3 = \frac{1}{\rho_3 c_3}(|P_3^+|^2(1+M_3)^2 - |P_3^-|^2(1-M_3)^2). \tag{20}$$

This was then normalized to the incident acoustic intensity I_1^+ at the inlet of the expansion chamber, where $I_1^+ = |P_1^+|^2(1+M_1)^2/\rho_1 c_1$, to obtain the relative acoustic power flux as both pipe areas are the same. Figure 13 shows the results for the normalized acoustic power flux in the outlet pipe for the first four order components with a Mach number of 0·1.

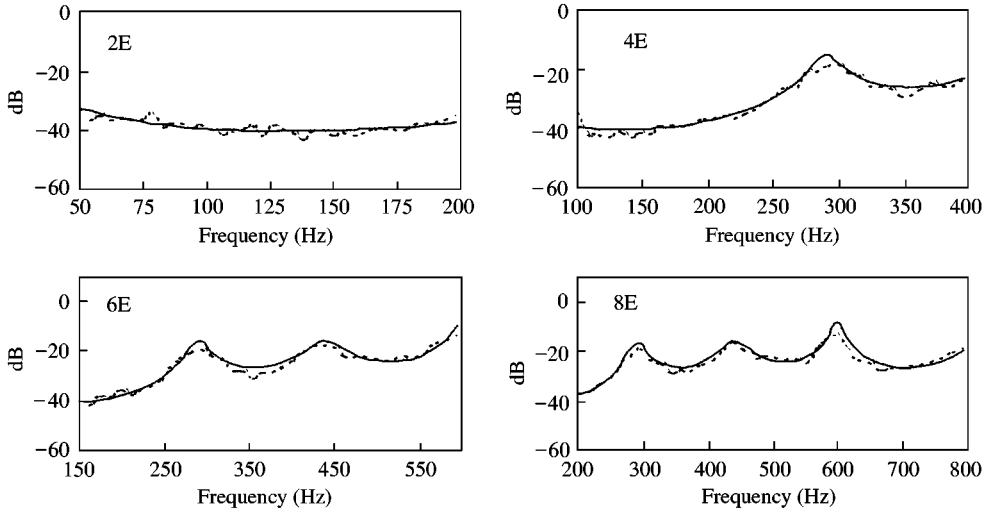

Figure 14. Measured (dash) and predicted (solid) normalized acoustic radiated power with a Mach number of 0·1.

The acoustic radiated power was estimated from the equation [17]

$$W_r = \frac{4\pi r^2 |G_{5,5}|^2}{\rho_0 c_0}, \tag{21}$$

where, r is the microphone radius, $G_{5,5}$ is the auto-spectrum at station $\#5$, while ρ_0 and c_0 are the ambient speed of sound and ambient density of air respectively. The acoustic radiated power was also normalized to the acoustic power flux at the inlet of the expansion chamber to obtain the relative radiated power. Figure 14 shows the predicted and measured radiated power for the first four order components with a Mach number of 0·1.

A fairly large measurement error due to contamination by non-acoustic pressure fluctuations can be tolerated in the resulting transfer function estimates as the results are directly estimated from the magnitudes of the measured acoustic spectral pressure ratios. This is illustrated by the excellent agreement between the measured and predicted results for the transfer function $H_{3,1}$ (see Figure 10) even at frequencies where the signal-to-noise ratios where relatively low for the $8E$ component between 500 and 600 Hz at station $\#3$ (see Figure 9). On the other hand, the system attenuation and acoustic power flux measurements are determined from the wave components and precise estimates of the corresponding cross-order spectra and transfer function order spectra are required to obtain reliable results. The raggedness for the system attenuation and acoustic power flux measurements between 500 and 600 Hz for the $6E$ and $8E$ components (see Figures 12 and 13) were caused by the lower signal-to-noise ratios, where the measured quantities were not sufficiently precise. The raggedness of the transfer function $H_{1,5}$ (Figure 11) and the acoustic radiated power (Figure 14) are partly due to room effects [1, 7] as an external microphone is required for these measurements.

Close inspection of the results reveal that, as one would expect, the levels of the four orders for each individual measurement are the same where the frequency span of the orders overlap. This is due to the fact that all the measured and predicted harmonic components are subjected to the same mass flow and temperature conditions for the complete sweep and the fact that all the results are either relative or normalized. It is, however, important to

realize that the frequency range, sweep rate and measurement resolution for each order must be different at all the overlapping frequencies.

4. VEHICLE MEASUREMENTS AND PREDICTIONS

The primary aim of the measurement technique is to asses the acoustic behaviour of a silencer component, together with all the variable factors for the transient operating conditions of a running engine. The measurement technique was applied to asses the acoustic performance of an expansion chamber fitted to the exhaust system of a Honda 1·5 l, four-stroke, four-cylinder engine for an acceleration run-up.

4.1. EXPERIMENTAL SET-UP

The vehicle was operated in third gear on a chassis dynamometer and the acceleration rate was controlled by means of software and hardware connected to the eddy current brake. The exhaust system lay out and the geometrical detail of the expansion chamber are displayed in Figure 15. Comparison with Figure 4 shows that the expansion ratio has been increased from 7·4 to 9, but the lengths are almost the same. A small packed perforated silencer is mounted at the front to reduce flow noise. The equipment set up is displayed in Figure 16.

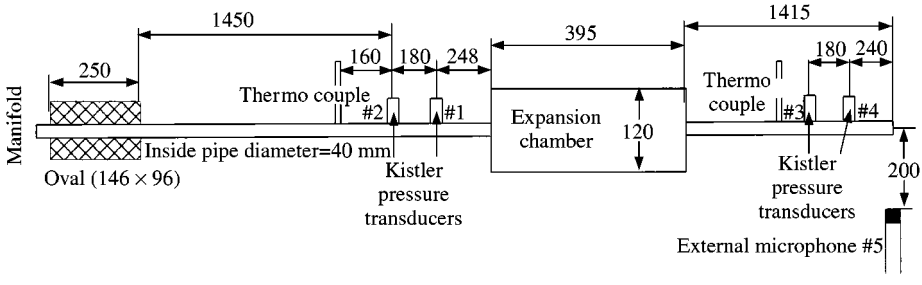

Figure 15. Exhaust system lay out for the Honda 1·5 l. All dimensions are in millimetres.

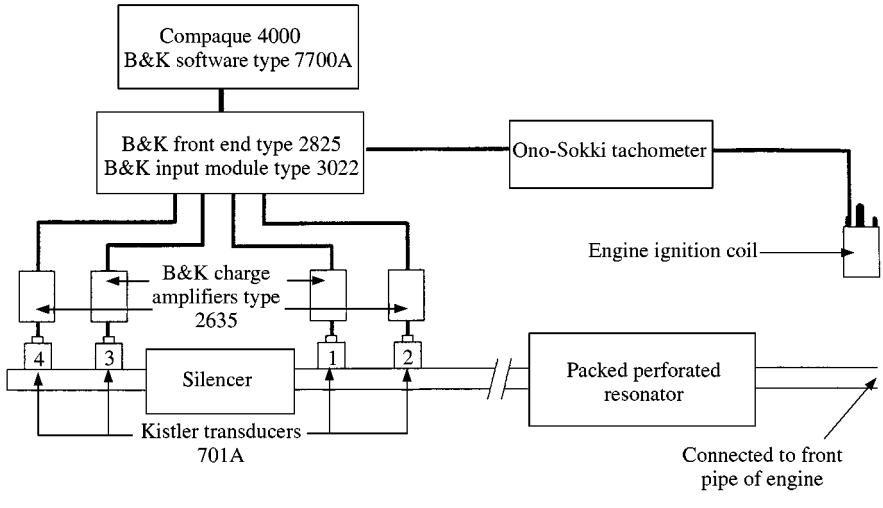

Figure 16. Experimental set-up used for the measurements on the vehicle.

The intake mass flow was measured with a hot wire probe that was connected to the inlet duct of the carburettor, mounted inside a 2 m long pipe to obtain a smooth flow. The exhaust mass flow was estimated from the intake mass flow. The exhaust gas temperature was measured with type K-thermocouples. An open hot junction with a 0·8 mm wire was used to obtain a fast response time. The wire was also mounted inside a ceramic sleeve to insulate it from the skin temperate of the exhaust system. The tracking of the fundamental frequency was measured with a tachometer, connected to the ignition coil of the vehicle. A data acquisition system was used to record the intake mass flow (kg/s), exhaust gas temperatures (°C), dynamometer speed (km/h), engine speed (r.p.m.) and wheel tracktive effort (N), at the same predetermined engine speed intervals anticipated for the acoustic measurements.

The Kistler (Type 701A) quartz pressure transducers used on the bench test were also used for the measurements on the vehicle. The effect of engine vibration on the sound pressure measurements was limited by the very low acceleration sensitivity of the transducers ($< 0{\cdot}001$ bar/g). The pressure transducers are mounted inside water cooled adapter, water was circulated through the adapters at ambient temperature. The installation of the transducers is displayed in Figure 3.

4.2. MEASUREMENT METHOD

The objective was to perform the measurements for the practical operating conditions of the engine. This implies a constant acceleration run-up for the speed range of the engine, while avoiding overheating of the engine. This was achieved for a sweep rate of 30 r.p.m./s in third gear from 1500 to 5400 r.p.m. Measurements performed at a slower sweep rate (15 r.p.m./s) required a cooling fan to avoid the engine overheating. The same signal processing parameters used for the bench test were used for the order tracking method namely 0·025 order resolution, 75% overlap and a Hanning window. However, only five averages could be achieved for a measurement interval of 120 r.p.m. (33 measurement intervals) and a sweep rate of 30 r.p.m./s. One recalls that an equivalent sweep rate of 15 r.p.m./s was used for the bench test measurements.

The wave decomposition calculation was performed with an extended version of the software program referred to in section 2.2. The program was designed in such a way that it calculated the wave components for each order from the measured harmonic order information and the corresponding variable mass flow and temperature.

4.3. ACOUSTIC PREDICTION

The variable mass flow and temperature gradients which were generated during the transient operating conditions of the engine have a controlling influence on the system acoustic performance. In order to incorporate these effect into the calculation process an additional module was added to the prediction code, APEX. The harmonic spectrum for each engine speed interval was calculated with the corresponding measured mass flow and temperature. The calculated harmonic spectra matrix was then manipulated to presented results in order format.

4.4. RESULTS AND DISCUSSION

The acoustic pressure field inside the exhaust system is contaminated by shear layer turbulence and flow noise due to the high flow velocities generated during the normal

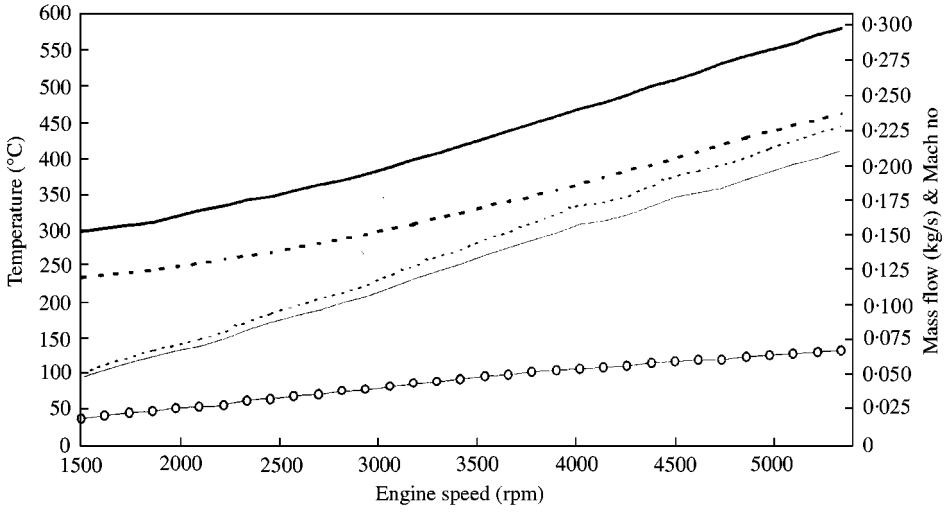

Figure 17. Mass flow (circles), inlet temperature (thick solid), outlet temperature (thick dash), inlet Mach number (thin dash) and outlet Mach number (thin solid) recorded for the Honda 1.5 l during a full throttle run-up on the chassis dynamometer.

operating conditions of an engine. This presents a formidable challenge to the performance of reliable measurements of the acoustic behaviour of the exhaust system elements. Figure 17 shows the mass flow, temperature and Mach number recorded at the inlet and outlet of the expansion chamber for a full throttle constant acceleration run-up (30 r.p.m./s). It can be noticed that the mass flow at maximum engine speed (0·07 kg/s) was the same as used on the bench; however, the increase in temperature and corresponding decrease in air density resulted in much higher flow velocities and therefore the maximum Mach number was increased by a factor of two ($M = 0{\cdot}2$). The order contour plot in Figure 18, measured at station $\#3$ gives an overview of the acoustic pressure field showing both the harmonic order information and random flow induced noise. The Y-axis represent engine speed, the X-axis represents the order number and the amplitude of the sound pressure is represented by the grey colour scale in decibels, order 1 refers to the $2E$ components and order 2 refers to the $4E$ component, etc. Low signal-to-noise areas can be identified where the harmonic orders approach the flow noise and the resonance frequencies of the tail pipe can be distinguished by the excitation of the order components and random flow noise around the hyperbolic curves. The sound pressure orders measured at station $\#1$ are displayed in Figure 19, where it can be observed that all the orders reached maximum levels above 165 dB (3556 Pa).

One problem associated with acoustic measurement on running engines is that it is not possible to measure the signal-to-noise ratio directly; this is due to the fact that it is not possible to determine the noise inside the system in the absence of the harmonic excitation. It was, however, important to establish an alternative method to estimate the signal-to-noise ratio for later explanation of certain recorded measurement errors and discrepancies. The basic approach was to estimate the value of the signal and of the noise independently by extracting the sum of the sound pressure spectral components from two different order bands positioned around the harmonic components. Thus, with reference to Figure 20, the signal-to-noise ratio is $P_a/(P_b - P_a)$, where, a is the order band from which the pressure for the signal was estimated and $(b - a)$ is the order band from which the pressure for the noise was estimated, while P_a and P_b are the corresponding sound pressure levels. For

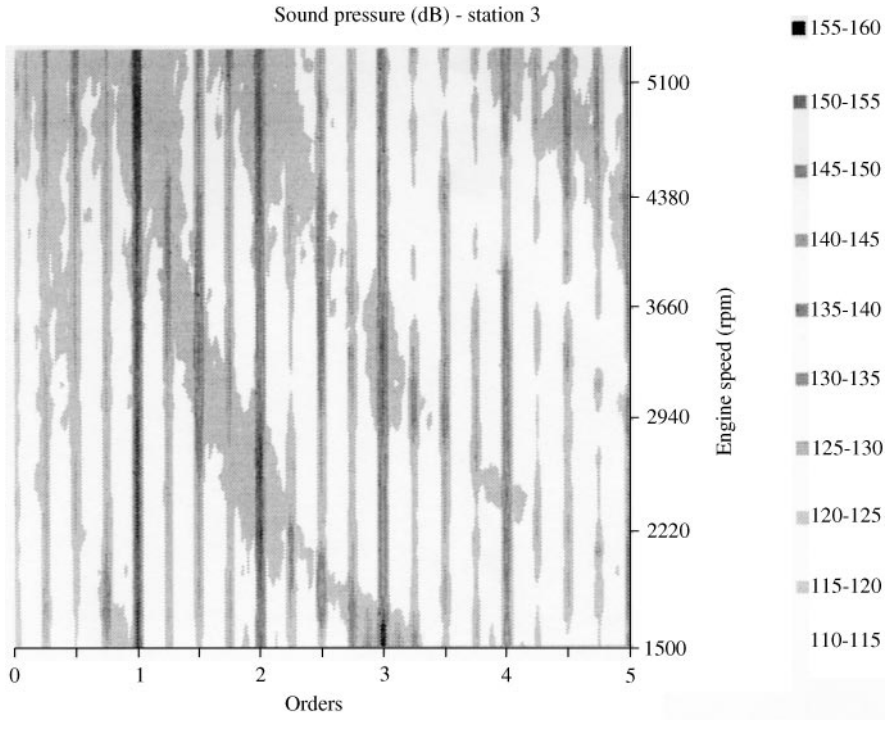

Figure 18. Order contour plot of the sound pressure at station #3 recorded for the Honda 1·5 l during a full throttle run-up on the chassis dynamometer.

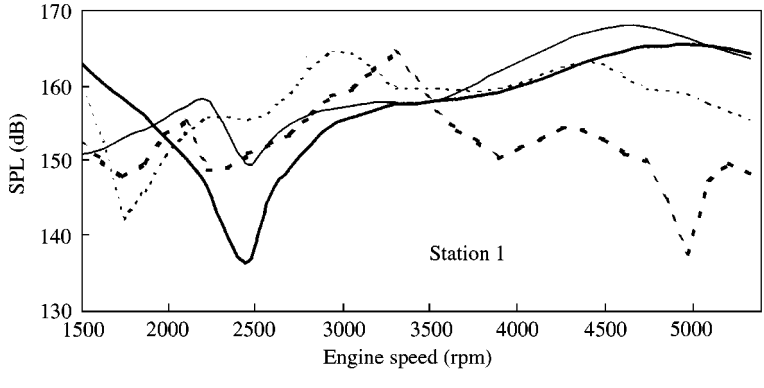

Figure 19. Sound pressure orders measured at station #1 for the Honda 1·5 l during a full throttle run-up on the chassis dynamometer; 2*E* (thick solid), 4*E* (thin solid), 6*E* (thin dash), 8*E* (thick dash).

example, Figure 20 shows the order spectrum recorded for station #3 (5100 r.p.m.) with the order bands for order 1 (2*E*). This method was optimized and then validated by comparing signal-to-noise ratios estimated as described above to actual measured signal-to-noise ratios on the bench.

The reliability of the measurements depends on a sufficiently precise estimation of the transfer functions at the inlet $H_{2,1}$ and the outlet $H_{4,3}$ of the silencer component. A sequence of measurements was performed over a period of time and it was found that measurement

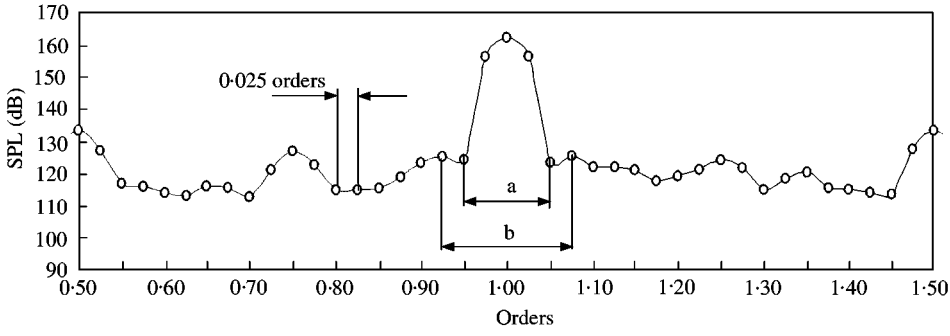

Figure 20. Order spectrum recorded for station #3 (5100 r.p.m.), displaying the order bands to estimate the signal-to-noise ratio for the first order (2*E*).

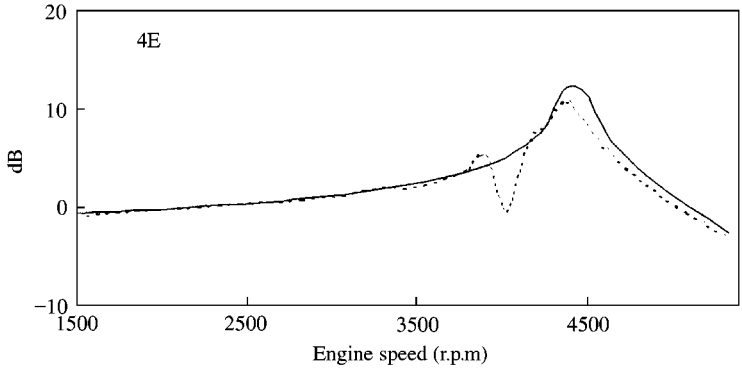

Figure 21. Measured (dash) and predicted (solid) transfer function (magnitude) $H_{4,3}$ of the 4*E* component with the transducers mounted close to the outlet side of the silencer.

error was in most cases related to the low signal-to-noise ratio at the outlet side of the silencer, resulting from the acoustic attenuation of the silencer in combination with the flow-induced pressure fluctuations at the outlet of the silencer as noted earlier with the flow bench. In order to improve the reliability of the measurements it was therefore necessary to optimize the position of the transducers at the outlet side to improve the signal-to-noise ratio. To illustrate such an example, the measured transfer function $H_{4,3}$ for the 4*E* component with the transducers mounted close to the silencer outlet in Figure 21 shows an apparently spurious spike at 4050 r.p.m., compared to good agreement between measured and predicted values shown in Figure 22, when the transducers were moved to the position as indicated in Figure 15. Note the significant change in both the measured and predicted spectral distribution at the two position along the same pipe. The results in Figure 23 clearly indicate that the measurement error resulted from low signal-to-noise ratios. These were below those found to yield acceptably realistic estimates of acoustic attenuation or acoustic power flux.

The predicted and measured acoustic performance of the expansion chamber after such precautions were adopted is shown in Figures 24–30. Good agreement was obtained between measured and predicted magnitude of the transfer functions at the inlet $H_{2,1}$ (Figure 24), the outlet pipe $H_{4,3}$ (Figure 25) and also for $H_{3,1}$ (Figure 26). Measured system attenuation (Figure 27) and normalized outlet power flux (Figure 28) also showed

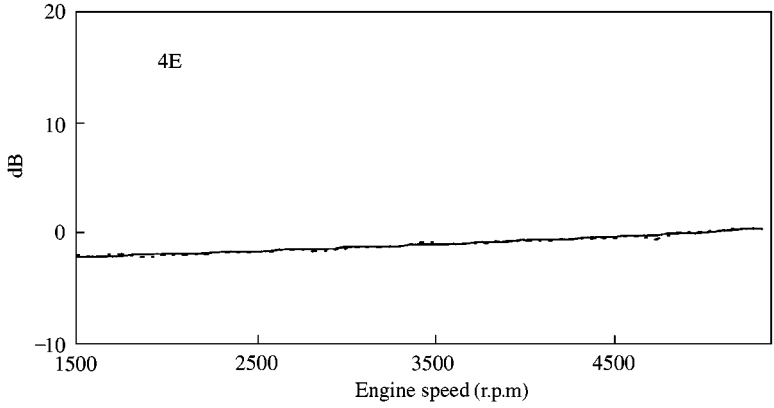

Figure 22. Measured (dash) and predicted (solid) transfer function (magnitude) $H_{4,3}$ of the 4E component with the transducers mounted close to the tail-pipe outlet.

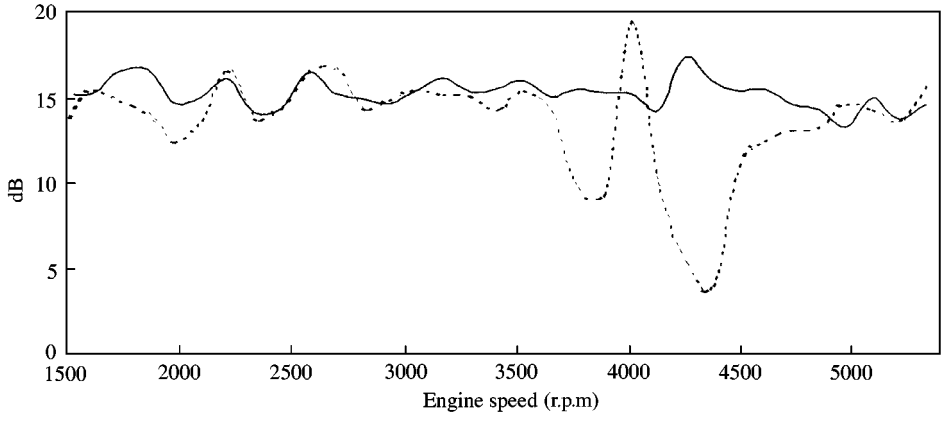

Figure 23. Signal-to-noise ratio estimated at station #3 with the pressure transducers mounted close to the outlet of the silencer (dash) and mounted close to the tail-pipe outlet (solid).

close agreement with predictions. Fair agreement was obtained between the measured and predicted normalized radiated power (Figure 29) and the corresponding transfer function $H_{2,5}$ (Figure 30). For these measurements it was assumed that the raggedness and the differences between measured and predicted results were partly due to room effects as an external microphone was used [1, 7]. Close identification of the differences between measurements and predictions lies in the future.

In most cases the small differences between measured and predicted results were due to lower estimates of the measured magnitudes at frequencies where maximum attenuation occurs. It can only be assumed that this was related, perhaps, to some other factors such as yielding of the silencer shell which was not correctly anticipated for in the theoretical models. However, in most cases close agreement was found between measured and predicted results; in particular, at resonance frequencies, that are obviously of much more practical significance in terms of the overall acoustic performance of the silencer component in service. The variable mass flow and temperature for the engine run-up on the test bed resulted in an amplitude variation and a frequency shift of the orders at corresponding

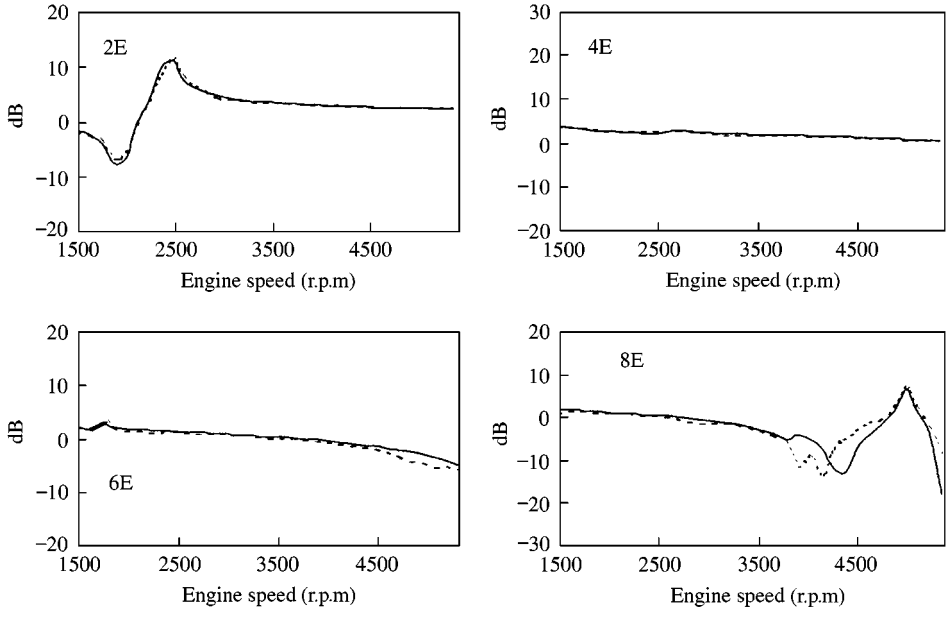

Figure 24. Measured (dash) and predicted (solid) magnitude of the transfer function (magnitude) $H_{2,1}$ for a full throttle run-up of the Honda 1·5 l.

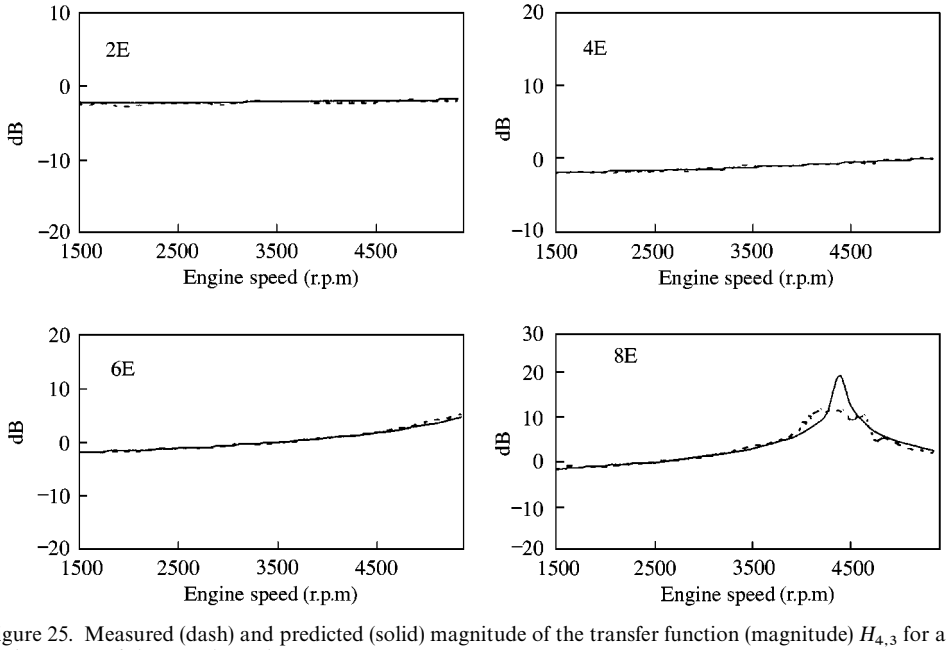

Figure 25. Measured (dash) and predicted (solid) magnitude of the transfer function (magnitude) $H_{4,3}$ for a full throttle run-up of the Honda 1·5 l.

frequencies. For example, in Figure 27 one can see that the first half wave resonance of the tail pipe was excited at 2580 r.p.m. (172 Hz, 1·1 dB) for the 4*E* component and at 1620 r.p.m. (162 Hz, −0·84 dB) for the 6*E* component.

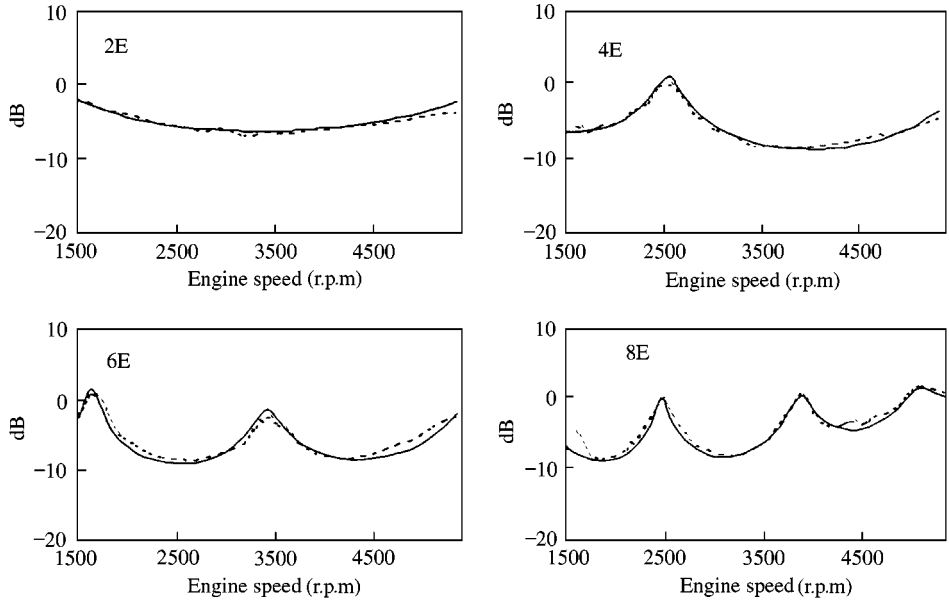

Figure 26. Measured (dash) and predicted (solid) magnitude of the transfer function (magnitude) $H_{3,1}$ for a full throttle run-up of the Honda 1·5 l.

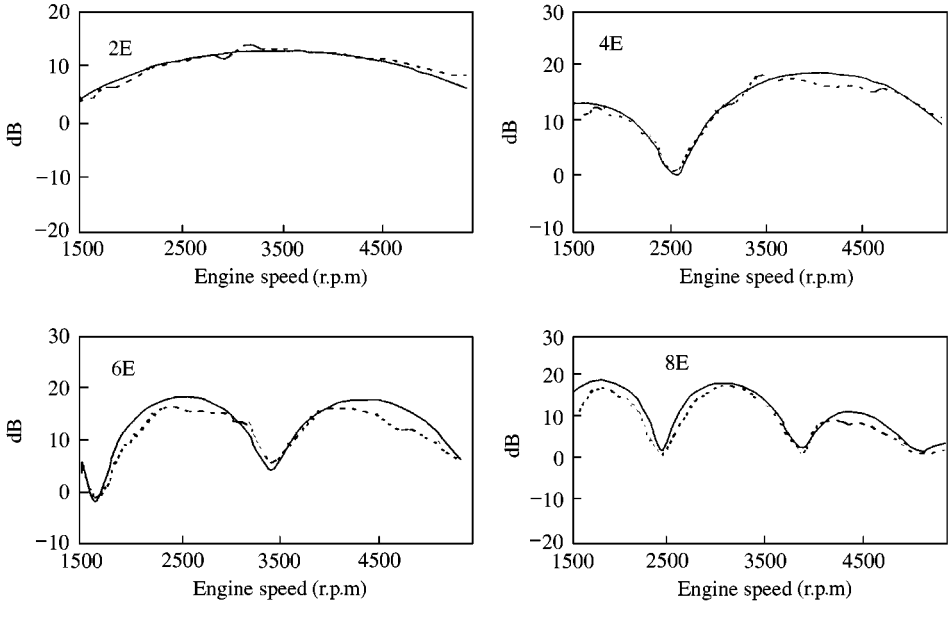

Figure 27. Measured (dash) and predicted (solid) system attenuation for a full throttle run-up of the Honda 1·5 l.

5. CONCLUSION

The bench test results showed that order analysis techniques can be used to capture transient harmonic pressure data to evaluate the acoustic performance of a silencer

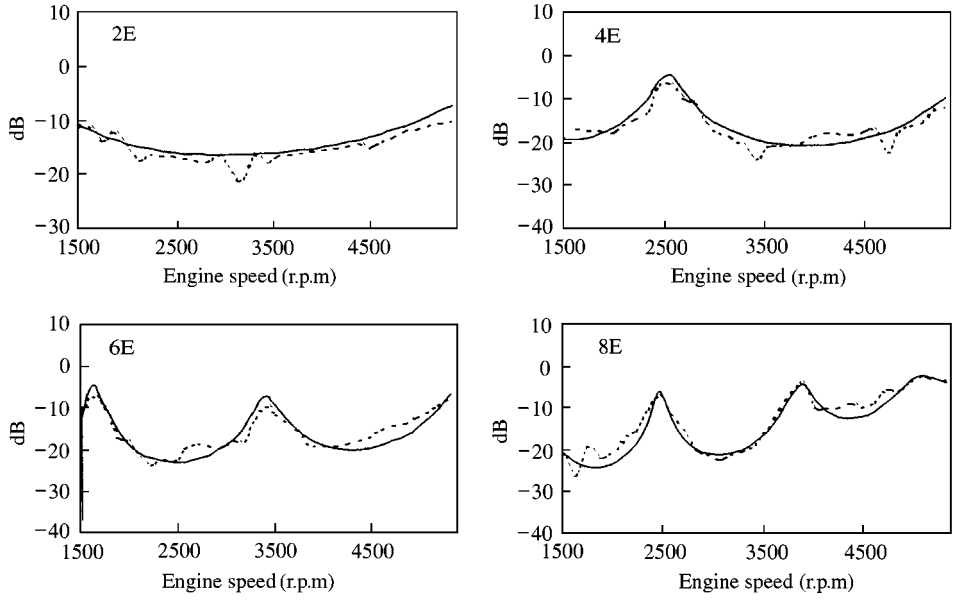

Figure 28. Measured (thin dash) and predicted (solid) normalized acoustic power flux in the outlet pipe for a full throttle run-up of the Honda 1·5 l.

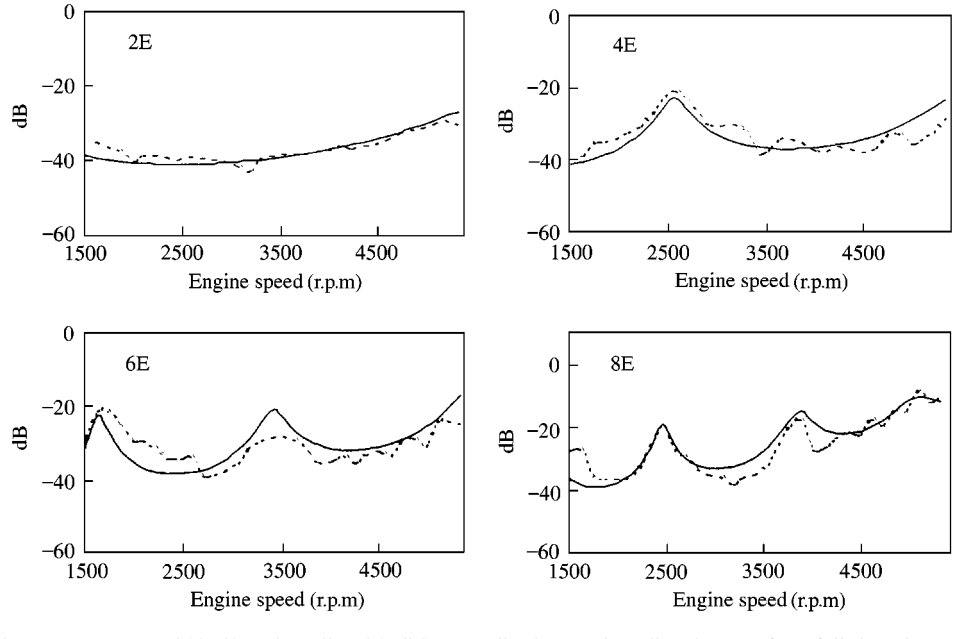

Figure 29. Measured (dash) and predicted (solid) normalized acoustic radiated power for a full throttle run-up of the Honda 1·5 l.

component. The analysis was performed with an order tracking method to eliminate leakage and to limit smearing. The signal-to-noise ratio and the coherence were improved when the analysis was performed with a higher order resolution and an increased number of

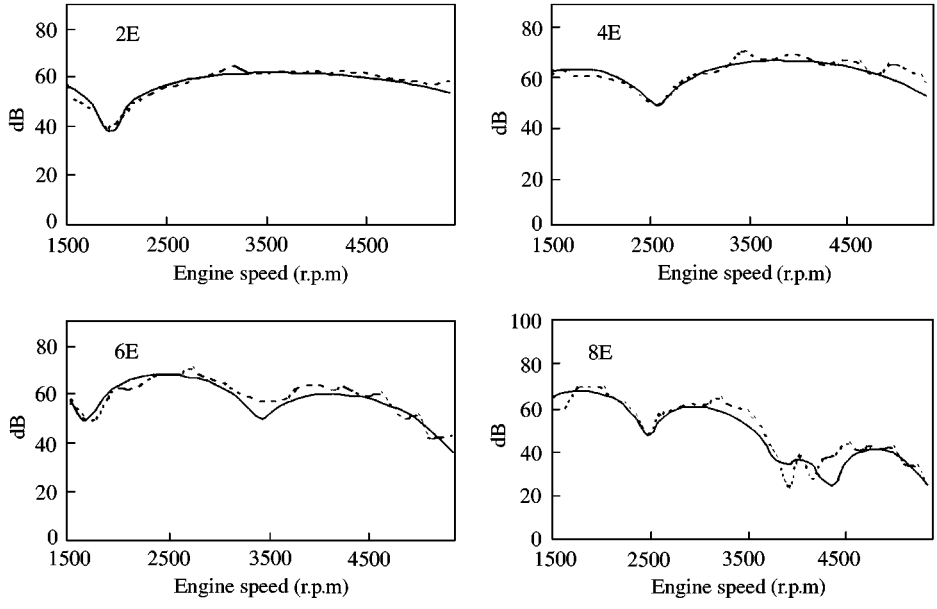

Figure 30. Measured (dash) and predicted (solid) magnitude of the transfer function $H_{2,5}$ for a full throttle run-up of the Honda 1·5 l.

averages. However, it was essential to ensure that the sampling rate was sufficient to compensate for the increasing sweep rates of the higher orders. Close agreement for the first four orders was found between predicted and measured acoustic transfer functions, system attenuation, acoustic power flux and acoustic radiated power which served to validate the measurement technique and opened the possibility to measure the acoustic performance of a silencer component on a running vehicle.

For the running engine the signal-to-noise ratios were estimated from the order spectra as it is not possible physically to measure them. Results showed that low signal-to-noise ratios in the tail pipe were mainly responsible for any measurement errors. In order to improve the reliability of the measurements the position of the pressure transducers at the outlet side of the silencer was optimized. In contrast to the bench test results, the orders for a particular acoustic quantity with overlapping frequencies showed amplitude variations and frequency shifts that were related to the variable mass flow and temperature. Measured and predicted acoustic attenuation and acoustic power flux at the outlet showed close agreement, while similar comparisons for radiated power showed fair agreement. Finally, the agreement between measurements and predictions calculated with the extended version of APEX indicates that linear acoustic theory remains valid for predicting wave propagation in the exhaust system of a running engines for high sound pressures up to 3500 Pa. This provides some justification for the adoption of appropriate Hybrid methods [17] for predicting the exhaust tail-pipe sound emission rather than those based on non-linear gas dynamic calculations [18].

The positive experimental results obtained on the running engine now open the possibility to measure the contribution of each individual element to the overall acoustic performance of a more commercial exhaust system. They also demonstrate the potential advantages to the acoustic design procedure compared with one based only on the evaluation of tail-pipe noise radiation measurements.

ACKNOWLEDGMENTS

The author gratefully acknowledge the advice and support of his tutor, Prof. P. O. A. L. Davies (ISVR). Thanks are also due to Dr P. Steenackers, Dr J. P. Janssens (BOSAL International, Belgium) and Dr K. R. Holland (ISVR) for their helpful ideas and discussions. This work was conducted at the Automotive research and development facility of BOSAL Africa and the author would like to thank BOSAL for their financial support.

REFERENCES

1. P. O. A. L. Davies and K. R. Holland 2001 *Journal of Sound and Vibration* **239**, 695–708. The observed aeroacoustic behaviour of some flow excited expansion chambers.
2. P. O. A. L. Davies and K. R. Holland 1999 *Journal of Sound and Vibration* **223**, 425–444. I.C. Engine intake and exhaust noise assessment.
3. R. J. Alfredson 1970 *Ph.D. Thesis, University of Southampton.* The design and optimisation of exhaust silencers.
4. R. J. Alfredson and P. O. A. L. Davies 1971 *Journal of Sound and Vibration* **15**, 175–196. Performance of exhaust silencer components.
5. J. E. Temple 1980 *M.Sc. Dissertation, University of Southampton.* An investigation into the source region characteristics of internal combustion engine exhaust systems.
6. E. A. Yaseen 1982 *M.Sc. Dissertation, University of Southampton.* Analysis of an exhaust system on a test bed.
7. P. O. A. L. Davies, K. R. Holland and D. Van der Walt 1999 *Noise and vibration seminar S*682 IMechE HQ. Sound power flux measurements in exhaust systems.
8. K. R. Holland and P. O. A. L. Davies 2000 *Journal of Sound and Vibration* **230**, 915–932. The measurement of sound power flux in flow ducts.
9. L. J. Eriksson 1980 *Journal of Acoustical Society of America* **68**, 545–550. Higher order mode effects in circular ducts and expansion chambers.
10. J. L. Bento Coelho 1983 *Ph.D. Thesis, University of Southampton.* Acoustic characteristics of perforate liners in expansion chambers.
11. P. O. A. L. Davies, M. F. Harrison and H. J. Collins 1997 *Journal of Sound and Vibration* **200**, 195–225. Acoustic modelling of multiple path silencers with experimental validation.
12. S. Gade, H. Herlufsen, H. Konstantin-Hansen and H. Vold 1995 *B&K Technical Review* No2. Characteristics of the Vold–Kalman order tracking filter.
13. D. K. Bandhopadhyay and D. Griffiths 1996 *SAE Paper* 951273. Methods for analyzing order spectra.
14. S. Gade, H. Herlufsen, H. Konstantin-Hansen and N. J. Wismer 1995 *B&K Technical Review* No2. Order tracking analysis.
15. R. B. Randall 1987 *Frequency analysis.* K. Larsen & Son; third edition, Denmark.
16. P. O. A. L. Davies 1988 *Journal of Sound and Vibration* **124**, 91–115. Practical flow duct acoustics.
17. P. O. A. L. Davies and M. F. Harrison 1997 *Journal of Sound and Vibration* **202**, 249–297. Predictive acoustic modelling applied to the control of intake/exhaust noise of internal combustion engines.
18. A. Onorati 1997 *Noise Control Engineering Journal* **45**, 35–51. Nonlinear fluid dynamic modelling of the reactive silencers involving extended inlet/outlet and perforated ducts.